Lithos 284–285 (2017) 171–179

Contents lists available at ScienceDirect

Lithos

journal homepage: www.elsevier.com/locate/lithos

Iron isotope fractionation during crustal anatexis: Constraints from migmatites from the Dabie orogen, Central China

Li-Juan Xu [a], Yongsheng He [a,*], Shui-Jiong Wang [b], Hongjie Wu [a], Shuguang Li [a,c]

[a] State Key Laboratory of Geological Processes and Mineral Resources, School of Earth Sciences and Mineral Resources, China University of Geosciences(CUGB), Beijing 100083, China
[b] Department of Earth and Atmospheric Science, Indiana University Bloomington, IN 47405, USA
[c] CAS Key Laboratory of Crust-Mantle Materials and Environments, School of Earth and Space Sciences, University of Science and Technology of China, Hefei 230026, China

ARTICLE INFO

Article history:
Received 4 September 2016
Accepted 4 April 2017
Available online 9 April 2017

Keywords:
Iron isotopes
Isotope fractionation
Migmatite
Crustal anatexis

ABSTRACT

Iron (Fe) isotope fractionation could occur during crustal melting, which may contribute to the isotopic variations of granites. Our current knowledge on Fe isotope fractionation during crustal melting remains rare. Thirteen leucosomes, 9 melanosomes and 1 amphibolitic schollen in 11 migmatites from the Dabie orogen, Central China were measured to investigate Fe isotope fractionation during crustal anatexis. The melanosomes and amphibolitic schollen yield δ^{56}Fe values from 0.018 ± 0.031‰ to 0.152 ± 0.027‰ with an average of 0.106‰. The leucosomes have δ^{56}Fe values from 0.107 ± 0.035‰ to 0.512 ± 0.028‰, variably higher than their coexisting melanosomes by 0.00 ~ 0.36‰. The δ^{56}Fe of leucosomes and melanosomes, as well as apparent isotope fractionation ($\Delta^{56}Fe_{L\text{-}M}$) between them, do not correlate with the abundance of crystalline carbonate, loss on ignition, and Th/U, indicating the insignificant effect of fluid components. High δ^{56}Fe values of three leucosomes (≥0.34‰), giving large $\Delta^{56}Fe_{L\text{-}M}$ from 0.22 to 0.36‰, were likely produced by feldspar accumulation, evidenced by their high Eu*, low FeOt/Al_2O_3 and high plagioclase abundance up to 50 vol%. Capture of peritectic amphiboles in another leucosome may explain its low $\Delta^{56}Fe_{L\text{-}M}$ ~0‰. After screening out these samples, 7 leucosome – melanosome pairs yield identical $\Delta^{56}Fe_{L\text{-}M}$ averaging 0.093 ± 0.056‰ (2SD, N = 7) within analytical uncertainties. No correlation between $\Delta^{56}Fe_{L\text{-}M}$ and Mg#, FeOt/Al_2O_3 or TiO_2/FeOt rules out the possibility that the fractionation observed here is produced by fractional crystallization and/or sub-solidus isotope re-equilibrium between leucosomes and melanosomes. Therefore, we suggest these consistent $\Delta^{56}Fe_{L\text{-}M}$ should record equilibrium Fe isotope fractionation during crustal anatexis producing these migmatites. The leucosomes and melanosomes have comparable $Fe^{3+}/\Sigma Fe$ ~ 0.40, and $\Delta^{56}Fe_{L\text{-}M}$ approximates 0.07‰ at $\frac{(Fe^{3+}/\Sigma Fe)_{leucosome}}{(Fe^{3+}/\Sigma Fe)_{menalosome}} = 1$. Fe isotope fractionation during crustal anatexis revealed here thus is not dominantly controlled by distribution of Fe^{3+} and Fe^{2+}, but by the difference in coordination number of iron between granitic melts and residual mafic minerals. The observation here argues that Fe isotope fractionation during crustal partial melting should also contribute to the previously revealed δ^{56}Fe variation in high silica granitic rocks.

1. Introduction

High silica (e.g., SiO_2 > 71 wt%) granitic rocks have a highly variable δ^{56}Fe from −0.04‰ to 0.46‰, which has been previously explained by isotope fractionation due to fluid exsolution, fractional crystallization, crustal melting, source heterogeneity and/or diffusion (Foden et al., 2015; Heimann et al., 2008; Poitrasson and Freydier, 2005; Schuessler et al., 2009; Sossi et al., 2012; Telus et al., 2012; Zambardi et al., 2014). Increasing evidence indicates that Fe isotopes fractionate during partial melting. For example, oceanic basalts have δ^{56}Fe values typically higher than the mean upper mantle by ~0.1‰ (Dauphas et al., 2009a; Teng et al., 2013; Weyer and Ionov, 2007). Fe isotope fractionation during mantle partial melting is commonly attributed to distribution of Fe^{3+} and Fe^{2+} between partial melts and their residua (Dauphas et al., 2009a, 2014; Teng et al., 2008, 2013; Weyer and Ionov, 2007), or explained by melting of mantle minerals (Williams and Bizimis, 2014). Our knowledge about Fe isotope fractionation that may occur during crustal partial melting remains rare, mainly due to the difficulty in reconstructing the source property and parental magma compositions for felsic igneous rocks, if considering the complexity of Fe isotope fractionation behavior during processes, e.g., fractional crystallization, after melt extraction (Foden et al., 2015; Konter et al., 2016; Telus et al., 2012; Teng et al., 2008).

Our limited knowledge about Fe isotope fractionation that may occur during crustal partial melting comes from data of migmatites in the Black Hills (Telus et al., 2012). Migmatites are a mixture of metamorphic rock and igneous rock (Marshak et al., 2009). They form via

* Corresponding author.
E-mail address: heys@cugb.edu.edu (Y. He).

http://dx.doi.org/10.1016/j.lithos.2017.04.005
0024-4937/

incipient partial melting in pre-existing gneisses, which is often induced by the breakdown of hydrous minerals (e.g., biotite) or influx of fluid (e.g., Clemens and Vielzeuf, 1987; Wang et al., 2013). Produced partial melts that are siliceous and hence not able to escape re-crystallize to form the igneous part of migmatites, which are generally quartz and feldspar rich and thus light-colored and called leucosomes. The residual part of migmatites are usually rich in dark-colored amphibole and biotite and called the melanosomes. Leucosome-melanosome pairs in migmatites thus may record the compositions of partial melts and their co-existing residuum during crustal anatexis. Telus et al. (2012) reported that the leucosomes from the Black Hills have δ^{56}Fe systematically higher than their associated melanosomes by 0.038 ± 0.056‰ ~ 0.196 ± 0.058‰, suggesting that significant Fe isotopic fractionation may also occur during partial melting of crustal lithologies. It should be noted, however, leucosomes may have experienced multiple processes during/after partial melting, e.g., the capture of peritectic minerals, fractional crystallization, and fluid exsolution (e.g. Wang et al., 2013), which all have the potential to change δ^{56}Fe of leucosomes. Care should be taken to evaluate if δ^{56}Fe of leucosomes observed can represent those values of partial melts in equilibrium to melanosomes during anatexis when using migmatites to study Fe isotope fractionation during crustal melting.

This study reports high precision Fe isotopic data for a suite of well-characterized migmatites from the Dabie orogen, central China (Wang et al., 2013). After a critical evaluation of potential isotopic effects of fluid influxion/exsolution, fractional crystallization, peritectic mineral capture, and subsolidus isotope re-equilibrium, detectable Fe isotope fractionation (Δ^{56}Fe ~ 0.09‰) during crustal anatexis that once occurred in these samples is identified. This suggests crustal partial melting as an important mechanism to produce the δ^{56}Fe variation observed in high silica granitic rocks.

2. Sample description

Migmatites used in this study are from the Dabie orogen (Fig. 1; Wang et al., 2013), a Triassic collision zone between the South China Block and the North China Block (e.g. Li et al., 1993, 2000). Petrology, geochronology, and geochemistry for these migmatites have been previously reported in Wang et al. (2013), and only the content relevant to this study is summarized below. The protoliths of Dabie migmatites used here are likely orthogneisses universal in the orogen. Large and euhedral amphibole grains present in the melanosome rim around leucosome and contain rounded inclusions of biotite + plagioclase + quartz, indicating growth of amphibole during partial melting of biotite + plagioclase + quartz. Lacking of anhydrous mafic minerals such as pyroxenes suggests that the anatexis occurred in the presence of a free fluid phase. Residual plagioclase can be identified in the melanosomes by its higher anorthite contents than the complementary leucosome parts. The melting reaction thus can be expressed as biotite + plagioclase + quartz + fluid ➔ granitic melt + amphibole + residual plagioclase. Based on Al-in-amphibole geobarometer (Schmidt, 1992) and geothermometer of co-existing amphibole and plagioclase (Holland and Blundy, 1994), this melting reaction may occur at P = ca.5.0 kbar, T = 705–744 °C (Wang et al., 2013). Migmatites measured here can be divided into three types: patch metatexites, stromatic metatexites, and diatexites based on their field structure. Patch metatexites are morphologically variable, and contain small, irregular leucogranitic patches (<0.2–0.5 cm across) with a volume fraction <10%. Stromatic metatexites contain 20–60 vol% leucosome layers (0.5–8 cm thick), and melanosomes constitute the rest volume and interlayer with leucosomes. Well-preserved layer structure indicates insignificant melt migration, and the leucosomes should represent re-crystallized partial melts in genetic link with their spatially associated melanosomes. Diatexites, composed of 0.5 cm–2 m wide leucosomes with coarse structure, were formed by increased folding and shearing. Large amphibole grains are present in the diatexitic leucosomes, and interpreted to be the peritectic products of melting reaction because of their poikilitic and porphyritic structures and rounded inclusions of biotite + plagioclase + quartz (Viruete, 1999; Wang et al., 2013). Amphibolitic blocks occur as schollen that seem to be unaffected by anatexis.

Melanosomes are mainly composed of amphibole (35–45%), biotite (30–40%), plagioclase (10–30%), K-feldspar (0–5%), and quartz (5–10%) with minor carbonates, Fe-oxides, zircon, and titanite. Carbonates are commonly found as interstitial phases in the melanosomes, suggesting the influx of a CO_2 rich fluid. The melanosome 0907 MSH-1A may have experienced the strongest metasomatism, evidenced by its high CaO up to 24.93 wt% and high Loss on Ignition up to 9.94 wt% (Wang

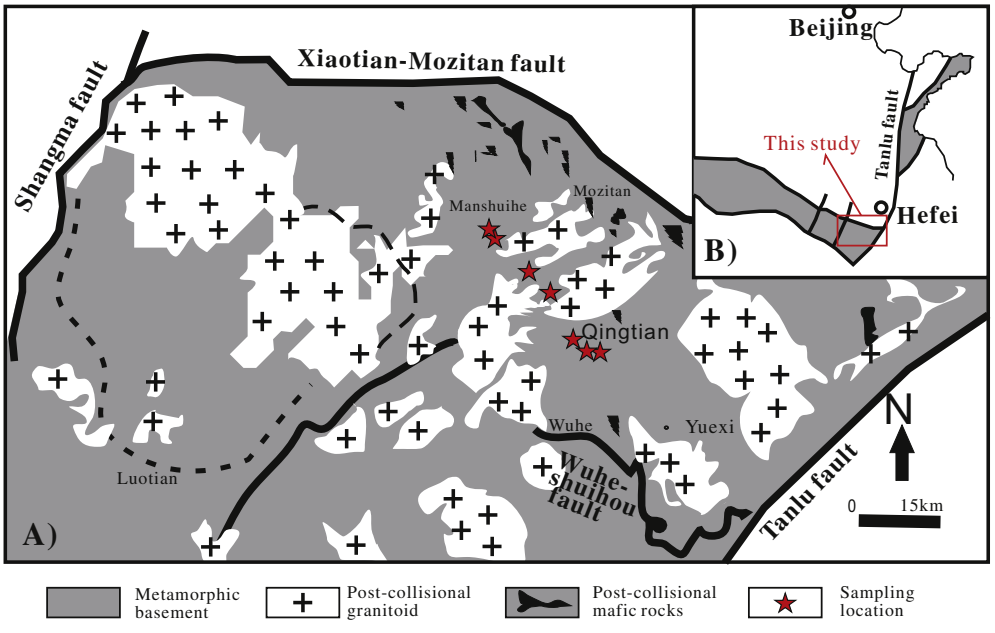

Fig. 1. Sampling location and simplified geological map of the Dabie orogen modified after Wang et al. (2013).

et al., 2013). One amphibolitic schollen 0909QT-4A was also measured here for comparison.

The leucosomes measured in this study can be divided into three types according to their petrology and geochemistry: i) the granitic leucosomes, ii) the trondhjemitic leucosomes, and iii) the leucosomes with captured peritectic amphibole. The first group leucosomes, mainly found in stromatic metatexites, are fined grained with typical granitic structure, and most likely represent re-crystallized partial melts of the local orthogneisses. They are composed of quartz (60–70%), k-feldspar (10–20%), plagioclase (10–20%), and biotite + amphibole (1–5%) as well as accessory carbonate, zircon, titanite, and Fe-oxides. The second group leucosomes, mainly trondhjemitic, appear as thin interlayers in stromatic metatexites or as irregular patches in patch metatexites. This type of leucosomes are relatively enriched in plagioclase (35–50%), and contain k-feldspar (1–5%), quartz (45–60%) and biotite (<1%) with minor zircon, titanite, and Fe-oxides. Substantial plagioclase accumulation is evidenced for these leucosomes by their positive Eu^* and Sr anomalies but depleted total REE contents. The third group leucosomes are from the diatexites, characterized by their coarse structure and the presence of large euhedral, peritectic amphibole grains.

Spatially associated leucosomes and melanosomes are defined here as the leucosome - melanosome pairs. For most of these pairs, the leucosome and the melanosome are in direct connection in the field before sampling. In some migmatites, e.g., 0907MSH 5-1 and 0907MSH 5, the first and second type of leucosomes co-exist in a hand specimen scale. According to the origins of leucosomes, the leucosome - melanosome pairs are noted hereafter as group I (re-crystallized melt), group II (cumulates), and group III (re-crystallized melt with captured amphibole), respectively.

3. Analytical techniques

Iron isotopic analyses were conducted in the Isotope Geochemistry Lab, China University of Geosciences Beijing after Dauphas et al. (2009b) and He et al. (2015), and only a brief description is summarized below. About 2.42–38.39 mg sample powders containing about 100 μg Fe were dissolved by concentrated HF—HNO_3—HCl—$HClO_4$. Fe was then purified with AG1X-8 (200–400mesh chloride form, Bio-Rad, USA) resin in a HCl medium. Matrix was removed by 8 ml 6 N HCl, and Fe was collected by 9 ml 0.4 N HCl. The same column chemistry was repeated twice. Whole procedure blank for Fe is <10 ng and thus considered negligible. The purified Fe was then measured on a Neptune Plus MC-ICPMS by standard-sample-bracketing, and Fe isotopic data are reported in traditional δ values relative to IRMM-014 ($\delta^{i}Fe = \left(\frac{(^{i}Fe/^{54}Fe)_{Sample}}{(^{i}Fe/^{54}Fe)_{IRMM014}} - 1\right) \times 1000$, where i can be 56 or 57). Each sample was typically measured for four times, and mean values as well as two standard errors are reported following Dauphas et al. (2009b). Accuracy and the long term reproducibility both are better than 0.05‰ for $\delta^{56}Fe$ under these conditions (He et al., 2015). Two international standards ($\delta^{56}Fe_{GSP-2} = 0.170 \pm 0.036‰$, $\delta^{56}Fe_{GSR-1} = 0.176 \pm 0.031‰$) were measured along with unknown samples, and yield results consistent with our long term mean values and those published by other laboratories (Table 1).

Table 1
Iron isotopic compositions of migmatites from the Dabie orogen.
Apparent isotope fractionation ($\Delta^{56}Fe_{L-M}$) of spatially associated leucosome-melanosome pairs is calculated. Data source for geological standards: a, He et al. (2015); b, Craddock and Dauphas (2010); c, Millet et al. (2012); d, Poitrasson and Freydier (2005). Superscript # denote two standard deviations.

Sample	Type	Classification	$\delta^{56}Fe$	2se	$\delta^{57}Fe$	2se	n	$\Delta^{56}Fe_{L-M}$	2se
Patch metaexite									
0907BJ-2-A	Melanosome		0.152	0.027	0.194	0.059	4		
0907BJ-2-B	Leucosome	Re-crystallized Melts'	0.143	0.027	0.210	0.059	4	−0.009	0.038
09GFA-2-A	Melanosome		0.121	0.027	0.203	0.059	4		
09GFA-2-B	Leucosome	Cumulates	0.337	0.027	0.494	0.059	4	0.216	0.038
Stromatic metatexite									
0907MSH-1-A	Melanosome		0.119	0.035	0.162	0.064	4		
0907MSH-1-B	Leucosome	Cumulates	0.263	0.035	0.353	0.064	4	0.144	0.050
0907MSH-4-A	Melanosome		0.018	0.031	0.028	0.068	4		
0907MSH-4-B	Leucosome	Cumulates	0.107	0.027	0.125	0.059	4	0.089	0.041
0907MSH-5-A	Melanosome		0.075	0.035	0.047	0.064	4		
0907MSH-5-B	Leucosome	Cumulates	0.160	0.035	0.229	0.064	4	0.086	0.050
0907MSH-5-C	Leucosome	Re-crystallized melts	0.175	0.035	0.249	0.064	4	0.100	0.050
0907MSH-5-A1	Melanosome		0.099	0.035	0.173	0.064	4		
0907MSH-5-B1	Leucosome	Cumulates	0.461	0.035	0.640	0.064	4	0.362	0.050
0907MSH-5-C1	Leucosome	Re-crystallized melts	0.201	0.035	0.245	0.064	4	0.101	0.050
0907MSH-6-A	Melanosome		0.082	0.027	0.128	0.059	4		
0907MSH-6-C	Leucosome	Re-crystallized melts	0.154	0.027	0.252	0.059	4	0.072	0.038
0907MSH-7-A	Melanosome		0.098	0.031	0.117	0.068	4		
0907MSH-7-C	Leucosome	Re-crystallized melts	0.153	0.027	0.201	0.059	4	0.056	0.041
Diatexite									
0907QT-1-A	Melanosome		0.191	0.035	0.287	0.064	4		
0907QT-1-B2	Leucosome	Cumulates	0.512	0.028	0.740	0.055	4	0.312	0.045
0907QT-4-A	Amphibolitic schollen		0.104	0.035	0.145	0.064	4		
0909QT-4	Leucosome	Re-crystallized Melts'	0.153	0.032	0.222	0.063	3		
0909QT-2-B	Leucosome	Re-crystallized Melts'	0.209	0.028	0.286	0.055	4		
Geostandards									
GSP-2			0.170	0.036	0.233	0.060	3		
Long-term mean[a]			0.157	0.025 #	0.222	0.038#			
Literature1[b]			0.153	0.038#	0.215	0.047#			
Literature1[c]			0.153	0.023#					
GSR-1			0.176	0.031	0.259	0.052	4		
Long-term mean[a]			0.148	0.047#	0.214	0.084#			
Literature[b]			0.173	0.023#	0.263	0.017#			
Literature[d]			0.170	0.040	0.243	0.049			

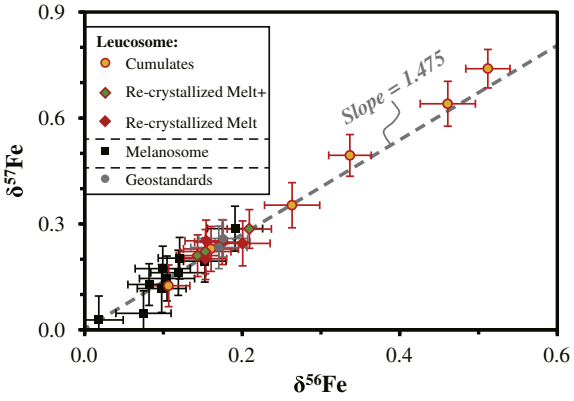

Fig. 2. $\delta^{57}Fe$ vs. $\delta^{56}Fe$ diagram. The results here are plotted along the theoretical mass dependent fractionation line (Young et al., 2002). Three types of leucosomes were measured in this study: the granitic leucosomes representing re-crystallized melts, the trondhjemitic leucosomes experienced substantial plagioclase accumulation (cumulates), and the granitic leucosomes with captured peritectic amphibole (re-crystallized melt+).

4. Results

Thirteen leucosomes, 9 melanosomes, and 1 amphibolitic schollen from 11 Dabie migmatites were measured in this study, and their Fe isotopic data are reported in Table 1 and plotted in the Figs. 2 and 3. The amphibolitic schollen 0907QT-4-A, enclosed in diatexites, yields a $\delta^{56}Fe$ of 0.104 ± 0.035‰, typical of intermediate igneous rocks (Fig. 3A). Melanosomes have variable $\delta^{56}Fe$ from 0.018 ± 0.031‰ to 0.152 ± 0.027‰ with an average of 0.106‰. The melanosome 0907MSH-1A with most abundant carbonate has a $\delta^{56}Fe$ of 0.119 ± 0.035‰, indistinguishable from the other melanosomes. $\delta^{56}Fe$ of leucosomes ranges from 0.107 ± 0.035 to 0.512 ± 0.028‰, systematically heavier than their spatially associated melanosomes. The trondhjemitic leucosomes with a plagioclase cumulate origin yield the largest $\delta^{56}Fe$ variation, from 0.107 ± 0.035‰ to 0.512 ± 0.028‰. By contrast, the other leucosomes have a relatively narrow range of $\delta^{56}Fe$, from 0.143 ± 0.027‰ to 0.209 ± 0.028‰. Apparent fractionation between each leucosome and its spatially associated melanosome is calculated and listed in Table 1. The $\Delta^{56}Fe_{L\text{-}M}$ values vary from −0.009 ± 0.038‰ to 0.362 ± 0.050‰, larger than the range previously revealed in migmatites from black hills (0.038 ± 0.056‰ to 0.196 ± 0.058‰; Telus et al., 2012).

5. Discussion

Highly variable $\Delta^{56}Fe_{L\text{-}M}$ are observed in the Dabie migmatites. A simple explanation might be Fe isotope fractionation during crustal anatexis. However, many other variables like fluid influxion/exsolution, fractional crystallization, mineral accumulation, and subsolidus re-equilibration, can also cause Fe isotope fractionation. Hereafter, we first assess whether the Fe isotopic systematics of these samples has been significantly affected by these processes and filter them accordingly to explore the Fe isotope fractionation scale during partial melting that once occurred in these migmatites.

5.1. Possible isotopic effect of fluid activities

Fluid exsolution during late stage magma crystallization may significantly increase $\delta^{56}Fe$ of high silica granites by extracting ferrous Fe that is enriched in light isotopes (Heimann et al., 2008; Poitrasson and Freydier, 2005). Based on the presence of carbonates and the absence of anhydrous mafic minerals, influx of a $H_2O + CO_2$ fluid has been proposed to trigger partial melting of protoliths of Dabie migmatites (Wang et al., 2013). All but one (0907MSH-1A that has abundant crystalline carbonates) leucosomes and melanosomes currently have low Loss on Ignition (LOI) (<2.0 wt%), indicating significant fluid exsolution during solidification. Therefore, it is necessary to evaluate if $\delta^{56}Fe$ of leucosomes and melanosomes measured here have been changed by fluid influx and exsolution.

Given the low FeOt contents of leucosomes relative to their associated melanosomes (e.g., $FeOt_L/FeOt_M \le 0.15$), $\delta^{56}Fe$ of melanosomes approximate the mean compositions of migmatites. As noted above, melanosome 0907MSH-1A, which may have experienced the strongest carbonate metasomatism, has a $\delta^{56}Fe$ close to the mean value of all melanosomes. Furthermore, no correlation can be identified between $\delta^{56}Fe$ and LOI for melanosomes. Therefore, it is unlikely that influx of a $H_2O + CO_2$ fluid has significantly changed the isotopic composition of the melting system. It is noted that melanosomes yield a detectable variation of $\delta^{56}Fe$ from 0.018 ± 0.031‰ to 0.152 ± 0.027‰, typical for terrestrial basaltic to andesitic igneous rocks (Dauphas et al., 2009a; Teng et al., 2013). Here, we attribute this $\delta^{56}Fe$ variation among melanosomes to the heterogeneity of their protoliths. To subtract the influence of protolith heterogeneity, hereafter we discuss if $\Delta^{56}Fe_{L\text{-}M}$ have been significantly changed by processes later than partial melting.

As to fluid exsolution, the extent of fluid exsolution was measured here by Th/U. K-feldspar and zircon, however, both have $D_U > 1$ and $D_U > D_{Th}$ (Bea et al., 1994; Rubatto and Hermann, 2007), and can also produce high Th/U ratios in their co-existing magmas. The maximum fractionation in Th/U during partial melting is estimated for Dabie migmatite, given by the most zircon and K-feldspar-rich residuum. Melanosomes measured here have Zr contents ≤177 ppm, suggesting residual zircon ≤0.4 wt%. Meanwhile, the abundance of K-feldspar is ≤5 vol%. Combined with these mineralogical constraints and available D_U and D_{Th} in the literature (Table 2), a batch partial melting model predicts that $\frac{(Th/U)_{melt}}{(Th/U)_{residuum}}$ shoud be no more than 4.5. Additional mechanisms thus are needed to explain the highly variable $\frac{(Th/U)_{leucosome}}{(Th/U)_{melanosome}}$ from 0.4 to 29 (Fig. 4). Fractional crystallization after partial melting could play a minimum role in increasing Th/U of the leucosomes, indicated by the low abundance of K-feldspar (≤5 vol%) and zircon (≤0.3 wt%) in the relevant cumulates and the low abundance of the cumulate phase itself in stromatic metatexites (Wang et al., 2013). High Th/U in the leucosomes representing re-crystallized melts are most likely resulted from fluid exsolution. U has a higher fluid-mobility than Th (Bali et al., 2009; Hawkesworth et al., 1997), and thus can be more readily transported by aqueous fluids. No detectable variation in $\Delta^{56}Fe_{L\text{-}M}$ (0.06–0.10‰) is identified for the group I leucosome-melanosome pairs with $\frac{(Th/U)_{leucosome}}{(Th/U)_{melanosome}}$ varying up to 29. Meanwhile, the other leucosome-melanosome pairs with variable $\Delta^{56}Fe_{L\text{-}M}$ (0.00–0.36‰) yield relatively low $\frac{(Th/U)_{leucosome}}{(Th/U)_{melanosome}}$ (0.4–5.1), comparable to the range predicted for melting processes. Therefore, we suggest insignificant Fe isotopic fractionation in these Dabie migamatites due to fluid exsolution.

5.2. Isotopic effects of fractional crystallization, accumulation, and peritectic amphibole capture

Differentiation during re-crystallization of the leucosomes is evidenced by the presence of light-colored cumulates (the second type leucosomes described in Section 2; details also referred to Wang et al. (2013)). These cumulates are enriched in plagioclase compared to other leucosomes representing re-crystallized melts, evidenced by their high plagioclase abundance and in consistency with their high Sr contents, high and positive Eu anomaly (Fig. 5A), as well as low REE contents (Wang et al., 2013). These cumulate samples display highly variable $\delta^{56}Fe$ ranging from 0.107 ± 0.027‰ to 0.512 ± 0.028‰, compared to the other leucosomes with $\delta^{56}Fe$ from 0.143 ± 0.027‰ to 0.209 ± 0.028‰ (Fig. 3A). The variable $\delta^{56}Fe$ of the cumulate samples cannot be attributed to the effect of magma compositions on Fe

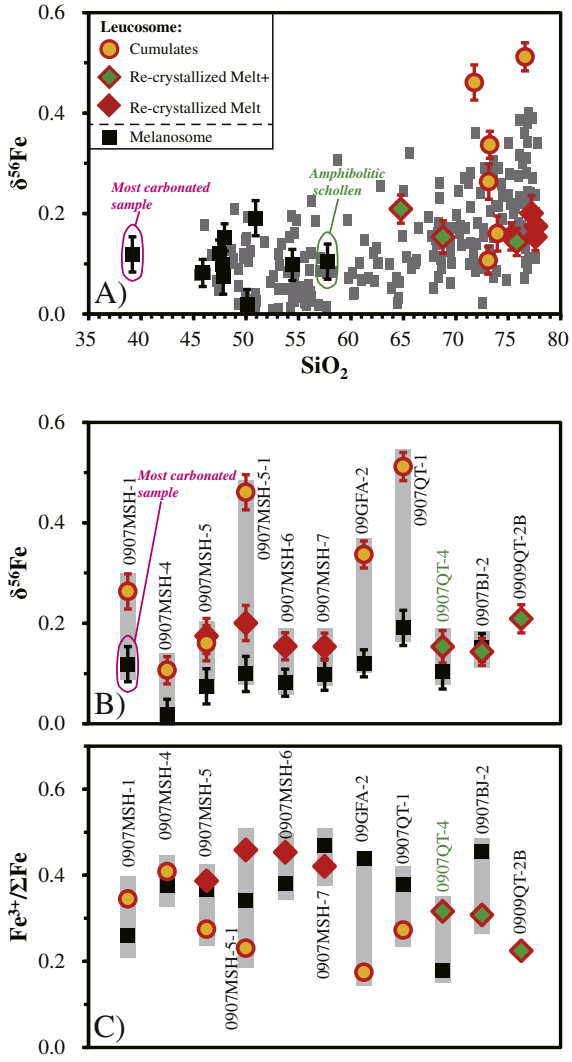

Fig. 3. δ^{56}Fe vs. SiO_2 diagram (A), and δ^{56}Fe (B) and $Fe^{3+}/\Sigma Fe$ (C) of spatially associated leucosome and melanosome pairs in migmatites from the Dabie orogen. It should be noted that the melanosome in 0907QT-4 is likely amphibolitic schollen, rather than represents residuum of melting reaction (Wang et al., 2013). Elemental data are from Wang et al. (2013).

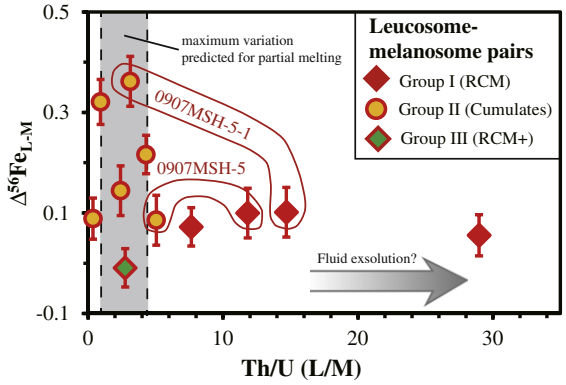

Fig. 4. δ^{56}Fe difference between spatially associated leucosome and melanosome ($\Delta^{56}Fe_{L\text{-}M}$) versus Th/U (L/M) diagram. Th/U (L/M) were calculated by $\frac{(Th/U)_{leucosome}}{(Th/U)_{melanosome}}$. Different symbols denote the pairs with different types of leucosomes. RCM is the abbreviation of Re-Crystallized Melts, and $^{+}$ denotes samples where captured peritectic amphibole is observed.

isotope fractionation, given that they are plotted off the global HSG trend* (Fig. S1). Instead, their variable δ^{56}Fe may be produced by feldspar accumulation, given that feldspar has δ^{56}Fe higher than its co-existing biotite by 0.56 ~ 1.33‰ in local granites (Wu et al., 2017). Feldspar has distinct low $FeOt/Al_2O_3$ (~0), when compared with biotite (1.26 ~ 1.38) and amphibole (1.48 ~ 2.15) (Wang et al., 2013). Thus, the whole rock $FeOt/Al_2O_3$ of leucosomes can be treated as an index of feldspar enrichment. The isotopic effect of feldspar accumulation is illustrated by a binary mixing between plagioclase and biotite (Fig. 5C). The calculation predicts that significant enhancement in whole rock δ^{56}Fe could occur, but only when plagioclase is very abundant and become a major Fe-bearing phase of the rock with a rather low whole rock $FeOt/Al_2O_3$, mainly due to the FeOt contents of plagioclase down to 0.07 wt% in high silica granites (Wu et al., 2017). As shown in Fig. 5, only 3 cumulate leucosomes with $FeOt/Al_2O_3$ ≤0.013 yield δ^{56}Fe substantially higher than all the other leucosomes, consistent with the prediction for the isotopic effect of feldspar accumulation. These 3 samples with $FeOt/Al_2O_3$ ≤0.013 will not be further considered, because their δ^{56}Fe have been likely changed by feldspar accumulation. Despite plagioclase has been suggested to be the main accumulating phase (Wang et al., 2013), subordinate accumulation of K-feldspar seems necessary to explain the relative high K_2O/Na_2O and (Na + K)/(Ca + Mg) of these 3 samples (Fig. S1). Accumulation or fractional crystallization of feldspar should have an insignificant effect on the other leucosomes, which is supported not only by the binary mixing calculation, but also evidenced by the leucosomes in 0907MSH-5. Both the cumulate layer and that representing re-crystallization melts co-exist in this sample. The cumulate, 0907MSH-5B, has a δ^{56}Fe of 0.160 ± 0.035‰ identical to that of the re-crystallization melt part (0.175 ± 0.035‰). This sample also provides an argument that the cumulate samples not extremely enriched in accumulated plagioclase with FeO/Al_2O_3 ≥0.018 can approximate their parental melts in terms of δ^{56}Fe.

Fractional crystallization of other Fe-bearing minerals is not evident by the petrology of Dabie migmatites (Wang et al., 2013), but its effect on Fe isotope fractionation is also evaluated by combining δ^{56}Fe and Mg# (Mg/(Mg + Fe) in mole fraction) data (Fig. 6). Fractional crystallization of ferrous Fe-enriched mafic minerals tends to increase δ^{56}Fe but decrease Mg# of residual melts, while magnetite crystallization has the opposite effect (Foden et al., 2015; Sossi et al., 2012). Save for one leucosome-melanosome pair in which the leucosome captures numerous peritectic amphibole grains, the leucosome-melanosome pairs yield nearly identical $\Delta^{56}Fe_{L\text{-}M}$ with an average of 0.093 ± 0.056‰ (2SD, N = 7). This is despite the variable Mg#(L-M) (the Mg# difference between leucosomes and their co-existing melanosomes, which is supposed to be changed during fractional crystallization) from −5.5 to −23. This indicates that

Table 2
U and Th partitioning data between minerals and high silica granitic magmas.
Data for zircon is from Rubatto and Hermann (2007) (800 °C). Those for biotite, plagioclase and K-feldspar are from Bea et al. (1994). Amphibole data are from GERM (https://earthref.org/GERM/). D_{Th} and D_U for quartz are estimated to be ~0. Superscript # denotes mineral abundance in a supposed residual mineral assemblage with the maximum potential to fractionate U and Th, indicated by the melanosome that has the most abundant zircon and K-feldspar.

Mineral	Zircon	Amphibole	Biotite	Plagioclase	K-feldspar	Quartz	Bulk D
D_{Th}	41	0.05	0.01	0.11	0.3	0	D_{Th} ~ 0.22
D_U	167	0.05	0.26	0.71	1.98	0	D_U ~ 0.98
Abundance#	0.4%	29.6%	30%	30%	5%	5%	D_{Th}/D_U (bulk) ~ 0.22

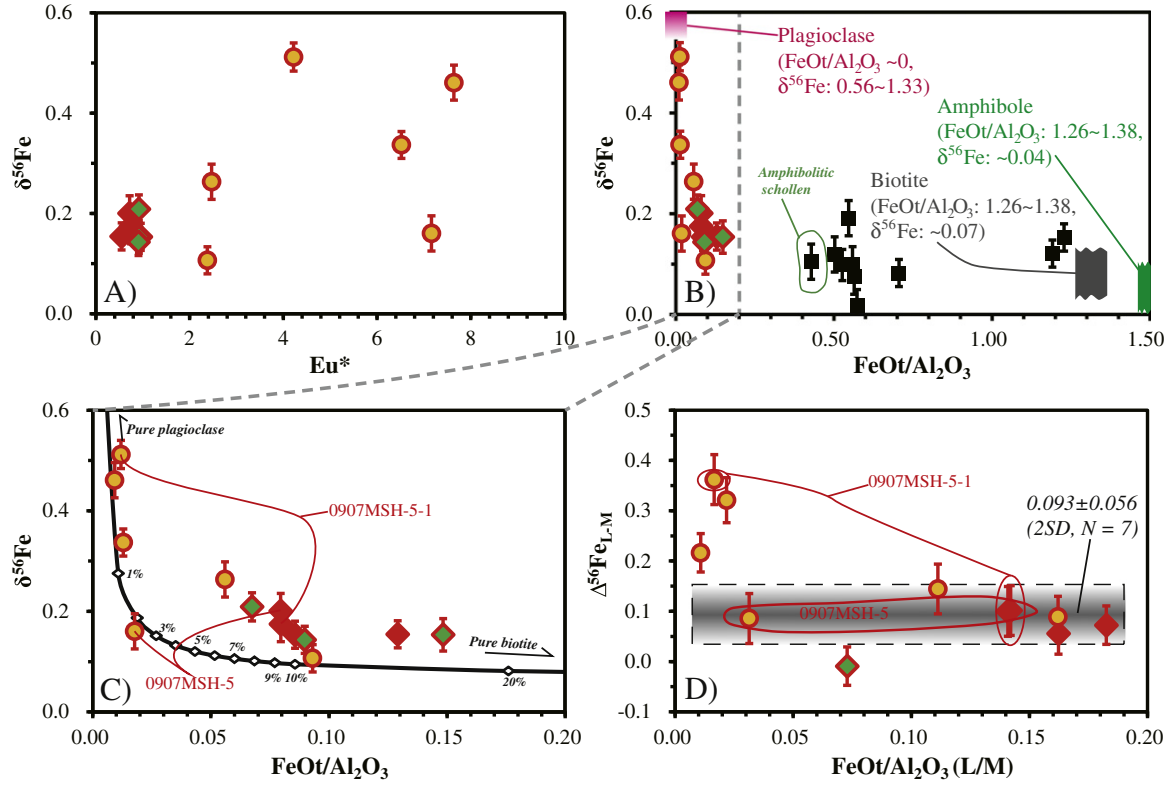

Fig. 5. $\delta^{56}Fe$ vs. Eu* (A), $\delta^{56}Fe$ vs. $FeOt/Al_2O_3$ (B and C) and $\Delta^{56}Fe_{L-M}$ vs. $\frac{(FeOt/Al_2O_3)_{leucosome}}{(FeOt/Al_2O_3)_{melanosome}}$ (D) diagrams. $Eu^* = Eu_N/\sqrt{(Sm_N \times Gd_N)}$, and subscript N represents normalization to the mean C1 Chondrite values (Sun and McDonough, 1989). FeOt is the abbreviation of total Fe content in the FeO form. The isotopic effect of plagioclase accumulation is approximated by a binary mixing curve between plagioclase (FeOt ~0.07 wt%, and Al_2O_3 ~ 24.80 wt%) and biotite (FeOt ~19.82 wt%, Al_2O_3 ~ 14.36 wt%) in Fig. 5C, where percentage numbers denote the fraction of biotite. Mineral elemental compositions are from Wang et al. (2013), except for the FeOt content of plagioclase that is assumed to similar to those values of plagioclase grains in local granites (Wu et al., 2017). $\delta^{56}Fe$ data of the amphibole, botite and plagioclase are from Heimann et al. (2008); Millet et al. (2012); Telus et al. (2012); and Wu et al. (2017). The mean $\delta^{56}Fe_{bio}$ available is used, and $\delta^{56}Fe$ of plagioclase in equilibrium is calculated using equations: $\Delta^{56}Fe_{plg\text{-}mag}$ (‰) = 0.0223 × Ab (mode%) − 1.15; $\Delta^{56}Fe_{bio\text{-}mag}$ (‰) = −1.16 × (Na + K)/Mg (in mole) + 0.557 (Wu et al., 2017).

fractional crystallization of other Fe-bearing minerals could be either insignificant or have a minimized effect on the Fe isotopic systematics of these seven Dabie migmatites, consistent with the petrology of Dabie migmatites (Wang et al., 2013).

Partial melts of intermediate rocks should have Mg# lower than their residua (Patino Douce, 2005). If the leucosomes in migmatites represent re-crystallized partial melts with the melanosomes as the refractory residua, the former should have Mg# lower than the latter. Indeed, the majority of leucosome-melanosome pairs here yield negative Mg#(L-M) (Fig. 6). The leucosome-melanosome pair 0907BJ-2, however, has positive Mg#(L-M), which can be attributed to the capture of numerous (up to 20%) peritectic amphibole grains in the leucosome (Wang et al., 2013). Binary mixing calculations indicate that addition of 20% peritectic amphibole that is assumed to have $\delta^{56}Fe$ similar to the melanosomes can reduce $\Delta^{56}Fe_{L-M}$ to an undetectable level. This may explain why $\Delta^{56}Fe_{L-M}$ of 0907BJ-2 (~0‰) is lower than those observed in the majority of leucosome-melanosome pairs.

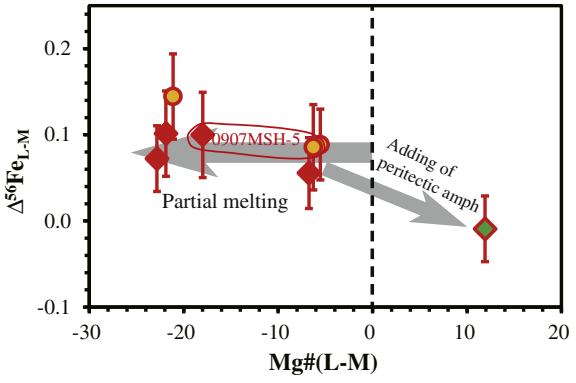

Fig. 6. $\Delta^{56}Fe_{L-M}$ vs. Mg# (L-M) diagram. Mg# (L-M) represents the Mg# difference between spatially associated leucosome and melanosome. Three pairs, where $\delta^{56}Fe$ of the leucosomes have been likely controlled by feldspar accumulation, are not plotted in this diagram.

5.3. Iron isotope fractionation during partial melting vs. mineral distribution

After screening out samples that may have been affected by plagioclase accumulation and capture of peritectic amphibole grains, 7 leucosome-melanosome pairs yield $\Delta^{56}Fe_{L-M}$ ranging from 0.056 ± 0.041‰ to 0.144 ± 0.050‰ with an average of 0.093 ± 0.056‰ (2SD, N = 7). We interpret these fractionations to reflect equilibrium partitioning given the fact that the seven leucosome-melanosome pairs yield identical fractionation within analytical uncertainties, over a 0.16‰ range in $\delta^{56}Fe$ values for the leucosomes (Fig. 7). This is supported by the magmatic equilibrium temperature (705–744 °C) recorded in co-existing amphibole and plagioclase (Wang et al., 2013). Equilibration in migmatites, however, may reflect mineral-mineral equilibrium among the leucosomes and their coexisting melanosomes, and accordingly the partitioning between them could reflect mineral distribution (e.g., Nabelek, 1999). Therefore, it is necessary to assess whether the isotope fractionation revealed here represents mineral-mineral equilibrium and mineral distribution between the leucosome - melanosome pairs. Iron is dominantly preserved in biotite and amphibole both in the leucosomes and the melanosomes. In addition, biotite has TiO_2/FeOt ~0.21 higher than amphibole (~0.10) (Wang et al., 2013).

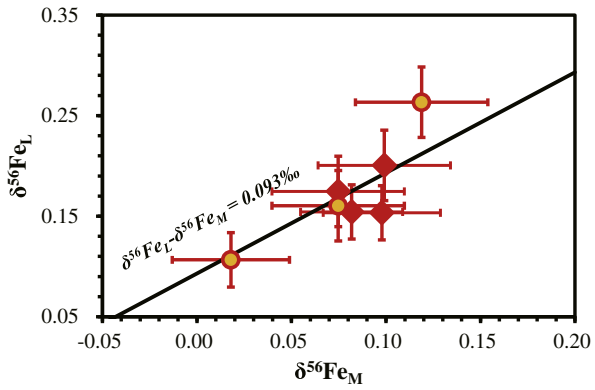

Fig. 7. $\delta^{56}Fe_L$ vs. $\delta^{56}Fe_M$ diagram. The samples likely affected by fractional crystallization and peritectic amphibole are not plotted here.

Accordingly, whole rock TiO_2/FeOt can reflect the proportion of biotite to amphibole in the samples. As shown in Fig. 8A, no correlation between $\Delta^{56}Fe_{L\text{-}M}$ and $\frac{(TiO_2/FeOt)_{leucosome}}{(TiO_2/FeOt)_{menalosome}}$ has been found. Therefore, the $\Delta^{56}Fe_{L\text{-}M}$ values measured here unlikely reflect mineral distribution, but could record Fe isotope fractionation during crustal anatexis instead. Main Fe pools as biotite and amphibole in the leucosomes are isolated by almost Fe-free quartz and feldspar, which may block mineral - mineral isotope equilibrium among leucosome - melanosome pairs.

Iron isotope fractionation during mantle partial melting has been extensively studied by measuring peridotites that have experienced melt extraction and comparing basalts to their sources, the upper mantle (Craddock et al., 2013; Dauphas et al., 2009a, 2014; Teng et al., 2013; Weyer and Ionov, 2007; Williams and Bizimis, 2014). Mantle peridotites that have experienced the more extensive melt extraction tend to have the lower $\delta^{56}Fe$ (Weyer and Ionov, 2007). Meanwhile, mid oceanic ridge basalts typically have $\delta^{56}Fe$ higher than the upper mantle by ~0.08‰ (Teng et al., 2013). Detectable Fe isotope fractionation thus occurs during mantle partial melting, which is commonly attributed to the preferential enrichment of Fe^{3+} in the melt and lower coordination and stronger bonding environment of Fe^{3+} compared to Fe^{2+} (Dauphas et al., 2009a, 2014). The migmatites studied here reveal that significant Fe isotope fractionation ~0.09‰ could also occur during crustal anatexis, which is largely consistent with the observed fractionation in the Black Hills migmatites (Fig. 9; Telus et al., 2012). It is interesting to note that, the leucosomes measured here, however, have $Fe^{3+}/\Sigma Fe$ ratios comparable to their coexisting melanosomes (Figs. 3C and 8B), likely due to the capability of residual amphibole and biotite to host Fe^{3+} in their crystal lattice. Despite an ambiguous positive trend is also observed between $\delta^{56}Fe_L$-$\delta^{56}Fe_M$ and $\frac{(Fe^{3+}/\Sigma Fe)_{leucosome}}{(Fe^{3+}/\Sigma Fe)_{menalosome}}$, a $\Delta^{56}Fe_{L\text{-}M}$ value ~0.07‰ at $\frac{(Fe^{3+}/\Sigma Fe)_{leucosome}}{(Fe^{3+}/\Sigma Fe)_{menalosome}} = 1$ and $(Fe^{3+}/\Sigma Fe)_{leucosome}$ = ca.0.40 indicates the observed Fe isotope fractionation during crustal anatexis is not dominantly controlled by the distribution of Fe^{3+} and Fe^{2+} between the melts and their residua. Based on nuclear resonant inelastic X-ray scattering and X-ray absorption near edge structure spectroscopy, Dauphas et al. (2014) has revealed that the force constants (⟨F⟩) of Fe^{3+}—O bonds in basaltic to dacitic glasses and both Fe^{2+} and Fe^{3+}—O bonds in rhyolitic glasses are higher than those in silicate and oxide minerals. Fe isotope fractionation during crustal anatexis thus

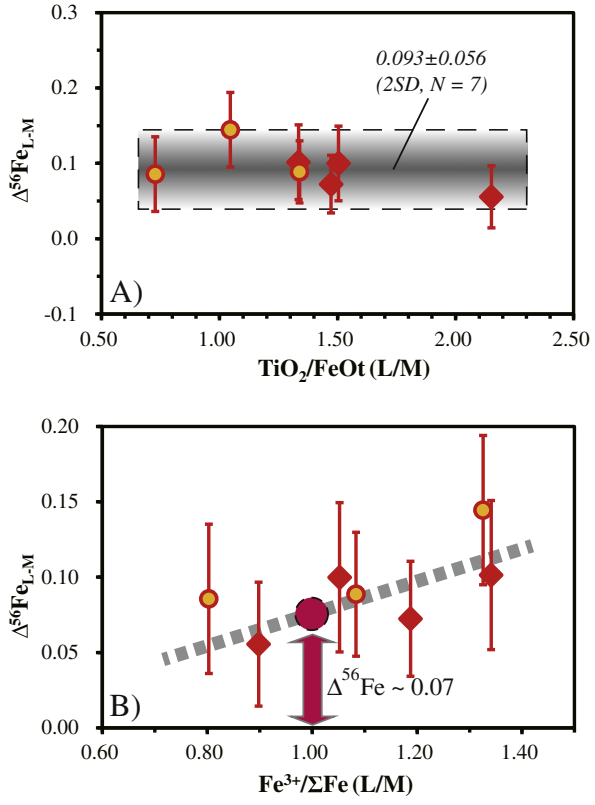

Fig. 8. $\Delta^{56}Fe_{L\text{-}M}$ vs. TiO_2/FeOt (L/M) (A) and $Fe^{3+}/\Sigma Fe$ (L/M) (B) diagrams. The samples likely affected by fractional crystallization and peritectic amphibole are not plotted here.

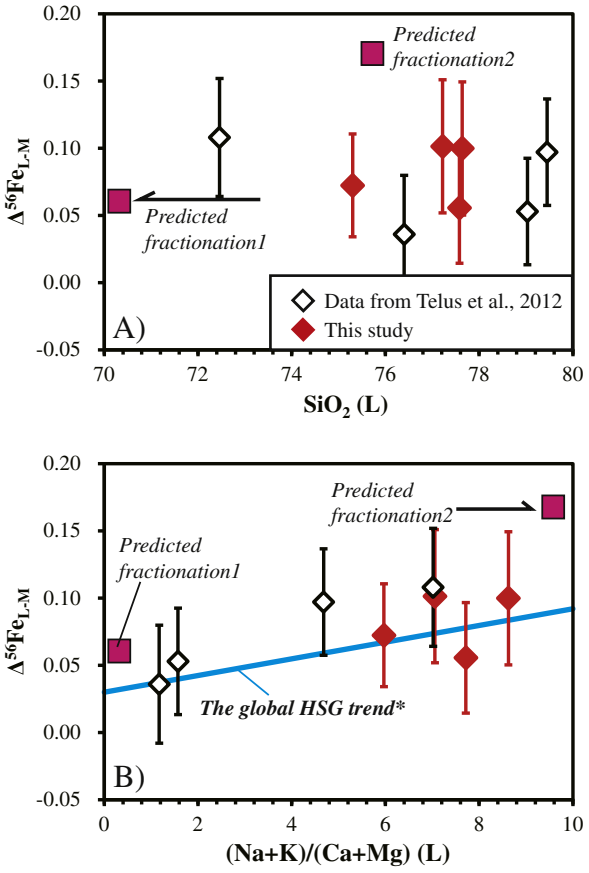

Fig. 9. Comparison of $\Delta^{56}Fe_{L\text{-}M}$ measured in this study with previous studies and theoretical prediction. The global high silica granite (HSG) trend, $\delta^{56}Fe$ (‰) = 0.0062 × (Na + K)/(Ca + Mg) + 0.130, is from He et al. (2017). To compare with $\Delta^{56}Fe_{L\text{-}M}$ measured here, the mean $\delta^{56}Fe$ of the upper continental crust from Foden et al. (2015) ~0.10‰ is substracted from the global HSG trend. Predicted fractionation factors are calculated based on force constants of Fe—O bonds in the melt and the residue with parameters listed in Table 3.

Table 3
Comparison of $\Delta^{56}Fe_{L\text{-}M}$ measured in this study with previous studies and theoretical prediction.
Migmatites from Telus et al. (2012) are also listed for comparison.
Note that one leucosome-melanosome pair (115–1) with an unusual leucosome composition, e.g., MgO = 4.85 wt% and TiO_2 = 3.84 wt% at SiO_2 = 74.91 wt%, is not included here. Superscript # and % denote that elemental data of leucosomes are shown. Predicted $\Delta^{56}Fe_{L\text{-}M}$ is calculated using mean force constants (⟨F⟩) at T = 724 °C and $(Fe^{3+}/\Sigma Fe)_{leucosome}$ = ca. 0.40 by: $\Delta^{56}Fe_{L\text{-}M} = 2853 \times \frac{\langle F\rangle_L - \langle F\rangle_M}{T^2}$ (T in kelvins; Dauphas et al., 2014). The mean force constants for basaltic to rhyolitic glasses are from Dauphas et al. (2014), and those for solid residue (dominantly determined by amphibole/biotite for crustal anatexis studied here) are assumed to be same to Fe^{2+}—O and Fe^{3+}—O in olivine and spinel respectively (Dauphas et al., 2014; Roskosz et al., 2015). The measured $\Delta^{56}Fe_{L\text{-}M}$ are consistent with the predicted value using mean force constants of basaltic to dacitic glasses, which implies that mean force constants of Fe—O in melts may be intrinsically controlled by (Na + K)/(Ca + Mg) (Dauphas et al., 2014; He et al., 2017; Sossi et al., 2012).

Phase name/samples	$SiO_2^{\#}$				
$(Na + K)/(Ca + Mg)^{\%}$	Mean force Constants				$\Delta^{56}Fe^{\$}_{L\text{-}M}$
	Fe^{3+}—O	Fe^{2+}—O			
Rhyolitic glasses	ca. 75.6 wt%	136–727	385	240	0.172‰
Basaltic to dacitic glasses	45.7–64.1 wt%	0.05–0.92	351	199	0.062‰
Solid residue	–	–	300	197	
Migmatites measured in this study	75.3–77.6 wt%	5.97–8.62			0.06–0.10‰
Migmatites from Telus et al. (2012)	72.5–79.5 wt%	1.17–7.02			0.04–0.11‰

may reflect the difference in Fe—O bonding conditions between the leucosomes typically with SiO_2 >73 wt% and residual mafic minerals.

The fractionation factor can be calculated based on mean force constants by $\Delta^{56}Fe_{L\text{-}M} = 2853 \times \frac{\langle F\rangle_L - \langle F\rangle_M}{T^2}$ (T in kelvins; Dauphas et al., 2014). Force constants of Fe—O bonds have not been reported yet for amphibole and biotite, which calls on future works. Assuming that amphibole and biotite have ⟨F⟩(Fe^{2+}—O) ~ 197 N/m and ⟨F⟩ (Fe^{3+}—O) ~ 300 N/m same to those in olivine and spinel (Dauphas et al., 2014; Roskosz et al., 2015), predicted $\Delta^{56}Fe_{L\text{-}M}$ at the melting temperature ~724 °C and $(Fe^{3+}/\Sigma Fe)_{leucosome}$ = ca.0.40 vary from 0.06‰ to 0.17‰ using ⟨F⟩ data for basaltic to dacitic glasses and rhyolitic ones from Dauphas et al. (2014), respectively (Table 3). The leucosomes studied here have SiO_2 similar to rhyolitic glasses but (Na + K)/(Ca + Mg) close to basaltic to dacitic glasses measured in Dauphas et al. (2014). Consistency of $\Delta^{56}Fe_{L\text{-}M}$ observed in this study with the predicted one using ⟨F⟩ data of basaltic to dacitic glasses not only supports that the measured $\Delta^{56}Fe_{L\text{-}M}$ here should record equilibrium Fe isotope fractionation during crustal anatexis, but also implies that force constants of Fe—O bonds in melts may be intrinsically controlled by alkalis rather than SiO_2 (Sossi et al., 2012; Dauphas et al., 2014; He et al., 2017).

5.4. General implications

Previous studies reveal that high silica granitic rocks (SiO_2 > 71%) have Fe isotopic compositions systematically heavier than those of more mafic igneous rocks (e.g., Poitrasson and Freydier, 2005). This phenomenon has been controversially attributed to processes, e.g., fluid exsolution (Heimann et al., 2008; Poitrasson and Freydier, 2005), fractional crystallization (Dauphas et al., 2014; Foden et al., 2015; Schuessler et al., 2009; Sossi et al., 2012; Telus et al., 2012), crustal melting (Foden et al., 2015; Telus et al., 2012), and diffusion (Zambardi et al., 2014; Zhu et al., 2015). Granites commonly have important contribution from crustal melting, except some A-type ones that have been explained as differentiated parts of mafic magmas (e.g., Foden et al., 2015; Turner et al., 1992). Migmatites measured here indicate that significant Fe isotope fractionation can occur during crustal melting, which must contribute to the $\delta^{56}Fe$ variation of granitic rocks. As noted above, Fe isotope fractionation during crustal melting could be dominantly controlled by the difference in Fe coordination environments between melts and residual minerals. Given that Fe—O bonds in high silica and alkalis granitic melts tend to be stronger than those in mafic to intermediate ones (Dauphas et al., 2014; Sossi et al., 2012), enhanced Fe isotope fractionation during crustal melting in the production of high silica and alkalis granitic rocks (SiO_2 > 71 wt%) may help to explain their relatively heavier Fe isotopic compositions. Crustal melting can serve as a mechanism alternative or complementary to prevailing models involving fluid exsolution, fractional crystallization and diffusion.

6. Conclusion

With a purpose to constrain isotope fractionation during crustal anatexis, Fe isotopic data are reported for 23 migmatite samples from the Dabie orogen, Central China. The leucosomes yield $\delta^{56}Fe$ higher than their coexisting melanosomes by 0 ~ 0.36‰. After screening out the samples that may be affected by fluid influx and exsolution, fractional crystallization, mineral accumulation, and capture of peritectic amphibole based on Th/U, FeOt/Al_2O_3, and Mg#, 7 leucosome-melanosome pairs yield consistent $\Delta^{56}Fe_{L\text{-}M}$ with an average of 0.093 ± 0.056‰ (2SD, N = 7). No correlation with $\frac{(TiO_2/FeOt)_{leucosome}}{(TiO_2/FeOt)_{menalosome}}$ suggests that these $\Delta^{56}Fe_{L\text{-}M}$ values may record isotope fractionation during crustal anatexis, rather than reflect subsolidus re-equilibrium. The leucosomes measured here have $Fe^{3+}/\Sigma Fe$ ratios comparable to their coexisting menalosomes. Fe isotope fractionation during crustal anatexis revealed here thus is not dominantly controlled by distribution of Fe^{3+} and Fe^{2+} between the melts and their residua. Instead, it can be explained by the difference in Fe-O bonding conditions between the granitic melts and their residual mafic minerals. The observation here thus suggests significant Fe isotope fractionation during crustal partial melting. Enhanced Fe isotope fractionation during crustal melting in the production of high silica and alkalis granitic rocks may help to explain their relatively heavier Fe isotopic compositions.

Supplementary data to this article can be found online at http://dx.doi.org/10.1016/j.lithos.2017.04.005.

Acknowledgement

The constructive comments from Dr. Paolo Sossi and efficient editorial handling of Dr. Chung Sun-Lin are greatly appreciated. This work is supported by the DREAM project of MOST China (2016YFC0600408) to YSH, the National Natural Science Foundation of China (No. 41403010 to LJX and No. 41473016 to YSH) and the Fundamental Research Funds for the Central Universities (No.292014064 to LJX and No.2652014056 to YSH). This is CUGB petrogeochemical contribution No.PGC-201521.

References

Bali, E., Audetat, A., Keppler, H., 2009. Mobility of U and Th in subduction zone fluids—a synthetic fluid inclusion study. Geochimica et Cosmochimica Acta 73 (13), A80.
Bea, F., Pereira, M.D., Stroh, A., 1994. Mineral/leucosome trace-element partitioning in a peraluminous migmatite (a laser ablation-ICP-MS study). Chemical Geology 117, 291–312.
Clemens, D.J., Vielzeuf, D., 1987. Constraints on melting and magma production in the crust. Earth and Planetary Science Letters 86, 287–306.
Craddock, P.R., Dauphas, N., 2010. Iron isotopic compositions of geological reference materials and chondrites. Geostandards and Geoanalytical Research 35 (1), 101–123.

Craddock, P.R., Warren, J.M., Dauphas, N., 2013. Abyssal peridotites reveal the near-chondritic Fe isotopic composition of the Earth. Earth and Planetary Science Letters 365, 63–76.
Dauphas, N., et al., 2009a. Iron isotopes may reveal the redox conditions of mantle melting from Archean to present. Earth and Planetary Science Letters 288 (1–2), 255–267.
Dauphas, N., Pourmand, A., Teng, F.-Z., 2009b. Routine isotopic analysis of iron by HR-MC-ICPMS: how precise and how accurate? Chemical Geology 267 (3–4), 175–184.
Dauphas, N., et al., 2014. Magma redox and structural controls on iron isotope variations in Earth's mantle and crust. Earth and Planetary Science Letters 398, 127–140.
Foden, J., Sossi, P.A., Wawryk, C.M., 2015. Fe isotopes and the contrasting petrogenesis of A-, I- and S-type granite. Lithos 212-215, 32–44.
Hawkesworth, C.J., Turner, S.P., McDermott, F., Peate, D.W., vanCalsteren, P., 1997. U-Th isotopes in arc magmas: implications for element transfer from the subducted crust. Science 276 (5312), 551–555.
He, Y., et al., 2015. High-precision iron isotope analysis of geological reference materials by high-resolution MC-ICP-MS. Geostandards and Geoanalytical Research 39 (3), 341–356.
He, Y.S., Wu, H.J., Ke, S., Liu, S.A., Wang, Q., 2017. Iron isotopic compositions of adakitic and non-adakitic granitic magmas: magma compositional control and subtle residual garnet effect. Geochimica et Cosmochimica Acta 203, 89–102.
Heimann, A., Beard, B.L., Johnson, C.M., 2008. The role of volatile exsolution and sub-solidus fluid/rock interactions in producing high 56Fe/54Fe ratios in siliceous igneous rocks. Geochimica et Cosmochimica Acta 72 (17), 4379–4396.
Holland, T., Blundy, J., 1994. Non-ideal interactions in calcic amphiboles and their bearing on amphibole-plagioclase themometry. Contributions to Mineralogy and Petrology 116, 433–447.
Konter, J.G., et al., 2016. Unusual δ56Fe values in Samoan rejuvenated lavas generated in the mantle. Earth and Planetary Science Letters 450, 221–232.
Li, S.G., et al., 1993. Collision of the North China and Yangtse Blocks and Formation of Coesite-Bearing Eclogites — timing and processes. Chemical Geology 109 (1–4), 89–111.
Li, S.G., Jagoutz, E., Chen, Y.Z., Li, Q.L., 2000. Sm-Nd and Rb-Sr isotopic chronology and cooling history of ultrahigh pressure metamorphic rocks and their country rocks at Shuanghe in the Dabie Mountains, Central China. Geochimica et Cosmochimica Acta 64 (6), 1077–1093.
Marshak, S., Wilkerson, M.B., Wilkerson, M.S., 2009. Essentials of Geology. Third edition. W. W. Norton & Company, pp. 1–996.
Millet, M.-A., Baker, J.A., Payne, C.E., 2012. Ultra-precise stable Fe isotope measurements by high resolution multiple-collector inductively coupled plasma mass spectrometry with a ^{57}Fe–^{58}Fe double spike. Chemical Geology 304-305, 18–25.
Nabelek, P.I., 1999. Trace element distribution among rock-forming minerals in Black Hills migmatites, South Dakota: a case for solid-state equilibrium. American Mineralogist 84, 1256–1269.
Patino Douce, A.E., 2005. Vapor-absent melting of tonalite at 15–32 kbar. Journal of Petrology 46 (2), 275–290.
Poitrasson, F., Freydier, R., 2005. Heavy iron isotope composition of granites determined by high resolution MC-ICP-MS. Chemical Geology 222 (1–2), 132–147.
Roskosz, M., Sio, C.K.I., Dauphas, N., Bi, W.L., Tissot, F.L.H., Hu, M.Y., Alp, E.E., 2015. Spinel-olivine-pyroxene equilibrium iron isotopic fractionation and applications to natural peridotites. Geochimica et Cosmochimica Acta 169, 184–199.
Rubatto, D., Hermann, J., 2007. Experimental zircon/melt and zircon/garnet trace element partitioning and implications for the geochronology of crustal rocks. Chemical Geology 241 (1–2), 38–61.
Schmidt, M.W., 1992. Amphibole composition in tonalite as a function of pressure: an experimental calibration of the Al-in-hornblende barometer. Contributions to Mineralogy and Petrology 110, 304–310.
Schuessler, J.A., Schoenberg, R., Sigmarsson, O., 2009. Iron and lithium isotope systematics of the Hekla volcano, Iceland — evidence for Fe isotope fractionation during magma differentiation. Chemical Geology 258 (1–2), 78–91.
Sossi, P.A., Foden, J.D., Halverson, G.P., 2012. Redox-controlled iron isotope fractionation during magmatic differentiation: an example from the Red Hill intrusion, S. Tasmania. Contributions to Mineralogy and Petrology 164 (5), 757–772.
Sun, S.S., McDonough, W.F., 1989. Chemical and isotopic systematics of oceanic basalts: implications for mantle composition and process. In: Saunders, A.D., Norry, M.J. (Eds.), Magmatism in the Ocean Basins. 42, pp. 313–345.
Telus, M., et al., 2012. Iron, zinc, magnesium and uranium isotopic fractionation during continental crust differentiation: the tale from migmatites, granitoids, and pegmatites. Geochimica et Cosmochimica Acta 97, 247–265.
Teng, F.-Z., Dauphas, N., Huang, S., Marty, B., 2013. Iron isotopic systematics of oceanic basalts. Geochimica et Cosmochimica Acta 107, 12–26.
Turner, S.P., Foden, J., Morrison, R.S., 1992. Derivation of some A-type magmas by fractionation of basaltic magma: an example from the Padthaway Ridge, South Australia. Lithos 28, 151–179.
Viruete, J.E., 1999. Hornblende-bearing leucosome development during syn-orogenic crustal extension in the Tormes Gneiss Dome, NW Iberian Massif, Spain. Lithos 46, 751–772.
Wang, S.-J., et al., 2013. Geochronology and geochemistry of leucosomes in the North Dabie Terrane, East China: implication for post-UHPM crustal melting during exhumation. Contributions to Mineralogy and Petrology 165 (5), 1009–1029.
Weyer, S., Ionov, D.A., 2007. Partial melting and melt percolation in the mantle: the message from Fe isotopes. Earth and Planetary Science Letters 259 (1–2), 119–133.
Williams, H.M., Bizimis, M., 2014. Iron isotope tracing of mantle heterogeneity within the source regions of oceanic basalts. Earth and Planetary Science Letters 404, 396–407.
Wu, H.J., He, Y.S., Bao, L.E., Zhu, C.W., Li, S.G., 2017. Mineral composition control on inter-mineral iron isotopic fractionation in granitoids. Geochimica et Cosmochimica Acta 198, 208–217.
Young, E.D., Galy, A., Nagahara, H., 2002. Kinetic and equilibrium mass-dependent isotope fractionation laws in nature and their geochemical and cosmochemical significance. Geochimica et Cosmochimica Acta 66, 1095–1104.
Zambardi, T., Lundstrom, C.C., Li, X., McCurry, M., 2014. Fe and Si isotope variations at Cedar Butte volcano; insight into magmatic differentiation. Earth and Planetary Science Letters 405, 169–179.
Zhu, D., Bao, H., Liu, Y., 2015. Non-traditional stable isotope behaviors in immiscible silica-melts in a mafic magma chamber. Scientific Reports 5, 17561.